# Fast-Curing Injectable Microporous Hydrogel for in Situ

# Cell Encapsulation

Seth D. Edwards,<sup>a</sup> Shujie Hou,<sup>a</sup> Jason M. Brown,<sup>a</sup> Ryann D. Boudreau,<sup>a</sup> Yuhan Lee,<sup>b</sup> Young Jo Kim,<sup>a</sup> Kyung Jae Jeong<sup>a</sup>\*

<sup>a</sup>Department of Chemical Engineering, University of New Hampshire, Durham, NH, 03824, United States.

<sup>b</sup>Engineering in Medicine, Department of Medicine, Center for Regenerative Therapeutics, Brigham and Women's Hospital, Harvard Medical School, Boston, MA, 02115, United States.

Keywords: injectable hydrogels, mesenchymal stem cell delivery, gelatin, tissue adhesion, antiinflammatory, microporous

#### **ABSTRACT**

Injectable hydrogels have previously demonstrated potential as a temporary scaffold for tissue regeneration, or as a delivery vehicle for cells, growth factors, or drugs. However, most injectable hydrogel systems lack a microporous structure, preventing host cell migration into the hydrogel interior and limiting spreading and proliferation of encapsulated cells. Herein an injectable microporous hydrogel assembled from gelatin/gelatin methacryloyl (GelMA) composite microgels is described. Microgels are produced by a water-in-oil emulsion using a gelatin/GelMA aqueous mixture. These microgels show improved thermal stability compared to GelMA-only microgels, and benefit from combined photopolymerization using UV irradiation (365 nm) in the presence of photoinitiator (PI) and enzymatic reaction by microbial transglutaminase (mTG), which together enable fast curing and tissue adhesion of

the hydrogel. The dual-crosslinking approach also allows for the reduction of PI concentration and minimizes cytotoxicity during photopolymerization. When applied for *in situ* cell encapsulation, encapsulated human dermal fibroblasts (hDFs) and human mesenchymal stem cells (hMSCs) are able to rapidly spread and proliferate in the pore space of the hydrogel. This hydrogel has the potential to enhance hMSC anti-inflammatory behavior through the demonstrated secretion of prostaglandin E2 (PGE2) and interleukin-6 (IL-6) by encapsulated cells. Altogether, this injectable formulation has the potential to be used as a cell delivery vehicle for various applications in regenerative medicine.

#### INTRODUCTION:

Injectable hydrogels are of high interest for use in regenerative medicine due to their high-water content and their ability to conform to the shape of surrounding tissue.<sup>1</sup> They have been used as a temporary matrix for tissue regeneration,<sup>2,3</sup> or as a delivery vehicle for therapeutic substances such as cells,<sup>4-6</sup> growth factors,<sup>7-9</sup> or small molecule drugs.<sup>10-12</sup> However, most injectable hydrogels do not possess large enough pores to allow for host cell migration into the hydrogel interior, as the hydrogel mesh size is on the order of nanometers. When applied for *in situ* cell encapsulation, encapsulated cells are trapped by the polymer chains delaying cell spreading and proliferation. Lowering the polymer concentration of the injectable hydrogel (lower than 5% w/v) will increase the gel mesh size, and can improve its interaction with cells,<sup>13-15</sup> but the mechanical stability of such gels can be significantly compromised.

One strategy to create pores in an injectable hydrogel is through injection and subsequent annealing of microgels. <sup>16–23</sup> Pores are formed by the interstitial space between adjacent microgels which allows for infiltration of host cells, and rapid spreading and proliferation of encapsulated cells. Such microporous hydrogels have applications in accelerated wound healing, <sup>24</sup> bone regeneration, <sup>25</sup> and *in situ* cell encapsulation for tissue engineering. <sup>26–30</sup> An optimal cell delivery vehicle should be capable of supporting a high concentration of cells, and facilitate interactions with the host tissue. Due to the high

internal growth area, and demonstrated improved retention of delivered cells *in vivo*, <sup>26</sup> assembled microparticle scaffolds are a promising approach for delivery of therapeutic cells.

Previously, we reported an injectable microporous hydrogel composed of gelatin microgels enzymatically crosslinked by microbial transglutaminase (mTG).<sup>31</sup> This novel formulation was injectable through a 26G needle, did not require any chemical modifications to the starting reagents, and the resulting microporous hydrogel facilitated the migration of surrounding cells to the hydrogel interior both *in vitro* and *ex vivo*, demonstrating its potential use in wound healing. This injectable formulation was also capable of *in situ* cell encapsulation, which resulted in rapid spreading and proliferation of encapsulated human dermal fibroblasts (hDFs) compared to the nonporous counterpart (**Figure S1**). However, the enzymatic crosslinking by mTG requires a long curing time (~ 30 min), which limits its suitability for clinical applications.

Presented herein is a rapidly curing microporous hydrogel composed of composite microgels that are made of gelatin and gelatin methacryloyl (GelMA). A microporous hydrogel can be formed within 2.5 minutes post injection by dual-crosslinking mechanisms – photopolymerization of GelMA and enzymatic crosslinking of unmodified gelatin by mTG (Figure 1). Photopolymerization of GelMA allows for rapid formation of bulk gel from microgel building blocks, while enzymatic crosslinking by mTG further stabilizes the hydrogel by forming additional covalent bonds between glutamine and lysine residues of gelatin and allows for tissue adhesion of the resulting hydrogel.<sup>32</sup> We demonstrate that this system enables the encapsulation of human primary cells, such as hDFs and human mesenchymal stem cells (hMSCs), with high viability and cell spreading. In addition, we examined the use of this hydrogel system for encapsulating MSCs primed by IFN-γ, demonstrating improved secretion of anti-inflammatory factors, which points to the potential use of this system for cell delivery to treat inflammatory diseases.

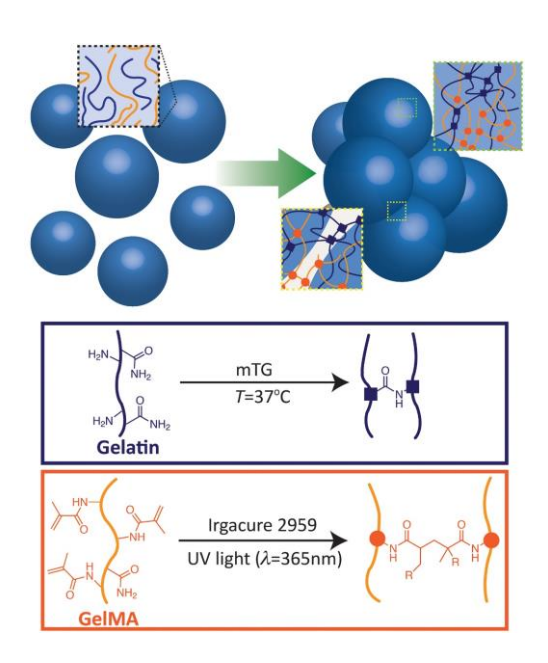


**Figure 1**. Schematic of the dual-crosslinking mechanisms of gelatin/GelMA microgels used to form a bulk hydrogel. A dual crosslinking approach is employed to rapidly cure microgels.

#### MATERIALS AND METHODS

#### Materials

All materials were purchased from Sigma-Aldrich (St. Louis, MO) unless specified. mTG was purchased from Ajinomoto (Fort Lee, NJ). Sterile phosphate buffer saline (PBS, pH 7.4), Dulbecco's Modified Eagle's Medium (DMEM), fetal bovine serum (FBS), and 10,000 U/ml penicillin/streptomycin (pen/strep) were purchased from Gibco (Carlsbad, CA). Human dermal fibroblasts (hDFs) were purchased from Lonza (Portsmouth, NH). Live/Dead Assay, Lactate Dehydrogenase (LDH) assay, and ActinRed 555 were purchased from Thermo Fisher Scientific (Waltham, MA). Fresh pig eyeballs were obtained from Visiontech (Sunnyvale, TX). Bone marrow derived hMSCs and media were purchased from Cell Applications (San Diego, CA). PGE2 and IL-6 ELISA kits were purchased from Abcam (Cambridge, MA).

#### Synthesis of Gelatin/GelMA Composite Microgels

The gelatin/GelMA composite microgels were prepared using a method similar to one previously described.<sup>31</sup> Due to the photoactive nature of GelMA, all procedures involving GelMA were performed

in the dark. A 2:1 mixture (by weight) of gelatin (type A, from bovine and porcine bones, bloom 300 g) and gelatin methacryloyl (bloom 300 g, 80% degree of substitution) was dissolved in 20 mL of deionized water at 50–55 °C to make a total 10% (w/v) aqueous solution. This solution was added dropwise to 200 mL of olive oil at 50–55 °C and stirred for 1 hour. The temperature of the mixture was lowered to reach room temperature for 30 min with stirring. Then the mixture was placed in an ice—water bath for an additional 30 min with stirring to solidify the microgels by inducing physical crosslinking. To precipitate the microgels, 100 mL of pre-cooled acetone (4 °C) were added to the mixture with stirring for 30 min in the ice—water bath. The microgels were separated from the olive oil and acetone by vacuum filtration and further washed with two 60 mL aliquots of precooled (4 °C) acetone. The microgels were immediately frozen at -80 °C, lyophilized, and kept dry until used. As a result of the separation of microgels using acetone, microgels have a very low water content when lyophilized, and microgel porosity was not seen to increase due to lyophilization.

# **Characterization of Microgels**

Microgels were visualized by scanning electron microscopy (SEM) (Tescan Lyra3 GMU FIB SEM, Brno, Czech Republic) and optical microscopy (EVOS XL, Life Technologies, Carlsbad, CA). Prior to the SEM imaging, lyophilized microgels were coated with gold/palladium to avoid charging. For quantification of hydrated microgel size distribution, 20 μL of a dilute microgel suspension in PBS was observed using an optical microscope. Size distribution of microgels was obtained from SEM and optical microscope images using ImageJ.

## **Bulk Hydrogel Formation**

Microporous hydrogels were made by mixing gelatin/GelMA composite microgels (10% w/v) with photoinitiator (PI) (Irgacure 2959) in PBS (0.5% or 0.05% w/v). Ascorbic acid was added to a final concentration of 0.005% (w/v) to minimize cytotoxicity during the UV irradiation.<sup>33</sup> This mixture was mixed with 20% (w/v) mTG in PBS in a 4:1 ratio. The final concentration of gelatin/GelMA polymer and mTG was 8% and 4%, respectively. UV light (365nm, ~35 mW/cm²) was applied for 2.5 mins to induce

photoinitiated crosslinking. Nonporous hydrogels were made using the same methods except that a gelatin/GelMA solution was used instead of gelatin/GelMA microgels.

## **Characterization of Hydrogels**

After the hydrogels were formed, their detailed structures were visualized with SEM. Prior to SEM imaging, the hydrogels were dehydrated through an ethanol series (30%, 50%, 60%, 70%, 80% and 90% once each, and then 100% twice) before being dried by critical point drying and coated with gold/palladium.

The viscoelastic properties of the hydrogels were characterized by rheometry (TA Instruments AR 550, New Castle, DE). A gelatin/GelMA microgel suspension was made in PBS containing PI and ascorbic acid as previously described. Crosslinking was initiated by mixing of mTG, and/or introduction of UV source. The gelation kinetics were observed at 37 °C, with an oscillatory stress of 1 Pa at 10 rad/s. Once gelation was completed, a frequency sweep was performed, increasing angular frequency from 0.1 to 100 rad/s with an oscillatory stress of 1 Pa at 37 °C. Then, temperature sweep was performed. Temperature was gradually increased from 5 to 45 °C with an oscillatory stress of 1 Pa at 10 rad/s.

The enzymatic degradation of microporous gelatin/GelMA hydrogels and gelatin/GelMA microgels was examined by incubating in collagenase type II solution (concentration = 0.5 U/mL) at 37 °C. At different time points (0h, 4h, 24 h), the hydrogels and microgels were collected, lyophilized, and weighed to calculate the fraction of remaining solids content.

### **Tissue Adhesion of the Hydrogels**

Porcine corneas were used to examine the tissue adhesion capability of the hydrogels. Corneas were collected from freshly obtained pig eyeballs using surgical scissors. A hole was created in the middle of the cornea using a biopsy punch (diameter = 8 mm) and was filled by injecting microgel solution prepared as previously described. After 2.5 min of crosslinking under different conditions, the tissue/hydrogel construct was immersed in a 45 °C warm water bath, to test for gelation and tissue adhesion.

#### **Cell Encapsulation and Characterization**

hDFs and hMSCs were cultured in T75 flasks using DMEM, supplemented with FBS and pen/strep or MSC growth medium, respectively. Cells of passage 3 were used for all experiments.

Prior to cell encapsulation, the gelatin/GelMA microgels were sterilized by incubation in 70% ethanol overnight, at 4 °C, then lyophilized before use. Gelatin, GelMA, mTG, Irgacure 2959, and ascorbic acid solutions were sterilized by syringe/vacuum filtration. For encapsulation, cells were mixed with microgel suspension or gelatin/GelMA solution in media, containing mTG, PI, and ascorbic acid, followed by 2.5 mins of UV irradiation. Hydrogels were then incubated at 37 °C for 1 hour. The encapsulated cells were cultured in the media described above.

The three-dimensional distribution of hDFs and hMSCs in hydrogel was visualized by confocal microscopy (Nikon A1R HD, Tokyo, Japan) on days 1 and 7 post-encapsulation using a live/dead cell viability kit, which stains living cells green (by calcein-AM) and dead cells red (by ethidium homodimer). To visualize the details of cell spreading and morphology inside the hydrogel, hDF samples were fixed in 4% paraformaldehyde (in PBS) overnight and stained with ActinRed 555. Z-stacked images were then obtained using the confocal microscope, and 2D projections were generated from Z-stacks using ImageJ. Sphericity, viability and proliferation were calculated using the plug-ins provided by ImageJ.

LDH assay was performed to assess cytotoxic effects related to the encapsulation process. hDFs seeded on well plates were used for maximum LDH controls, and hydrogels formed without encapsulated cells were used as negative controls. The culture media was removed on day 1 and 7 for analysis.

hMSCs were exposed to growth medium with IFN- $\gamma$  (50 ng/mL) for 24 hours before cell encapsulation. After encapsulation, cells were supplemented with growth medium, which was collected and frozen at -20 °C until use. The media was tested for secreted factors PGE2 and IL-6, using ELISA kits.

#### **Statistical Analysis**

All data is represented as means, and all error bars represent standard deviations. All experiments were run with at least n = 3 samples. Statistical significance was determined using a student's t-test when

comparing two groups, or Tukey's HSD post hoc test for experiments comparing more than two groups. P < 0.05 was considered statistically significant.

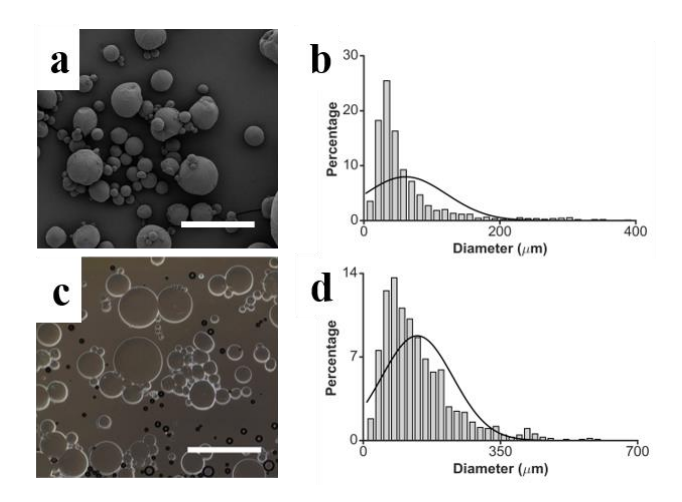


Figure 2. Composite microgel characterization. (a) SEM image of dry gelatin/GelMA microspheres. Scale bar = 200  $\mu$ m (b) Size distribution of dry microspheres. The average diameter = 61  $\pm$  60  $\mu$ m. (c) Optical micrograph of gelatin/GelMA microgels in PBS. Scale bar = 200  $\mu$ m. (d) Size distribution of swelled microgels. The average diameter = 139  $\pm$  90  $\mu$ m.

#### RESULTS AND DISCUSSION

Gelatin/GelMA microgels were produced using a 10% (w/v) aqueous mixture of unmodified gelatin and GelMA (80% substitution) at a 2:1 ratio by weight, in order to facilitate both enzymatic crosslinking by mTG and photocrosslinking by UV irradiation. A higher amount of gelatin than GelMA was used to make microgels in order to improve the thermal stability. A water-in-oil emulsion was created using this solution, which generated physically crosslinked polydisperse microspheres (**Figure 2**). The freeze-dried microgels were spherical in shape (Figure 2a) with an average diameter of 61 ( $\pm$  60)  $\mu$ m (Figure 2b). When equilibrated in an aqueous environment (Figure 2c), the average diameter increased to 139 ( $\pm$  90)  $\mu$ m due to swelling (Figure 2d). Based on this, the space between assembled microgels is on the order of tens of microns in size, which allows adequate space for encapsulation of human cells.

Microgel polydispersity is a result of batch manufacture of microgels; monodisperse microgels of gelatin/GelMA can be produced by the use of microfluidic devices. <sup>16,17</sup> Photo-curable microgels from a mixture of unmodified gelatin and GelMA have advantages over GelMA-only microgels, as the mixture can be cured also by enzymatic crosslinking, and thermal stability of microgels can be fine-tuned by adjusting the gelatin/GelMA ratio. For example, previously described microgels that are made by GelMA only (80% substitution) are unstable at room temperature and the curing has to be done using chilled solutions, <sup>17</sup> which is not an ideal condition for *in situ* cell encapsulation. High-substitution GelMA microgels can be partially UV cured to improve stability, <sup>34</sup> but this solution creates a tradeoff between stability and hydrogel gelation that is not necessary when using composite microgels. Composite microgels are stable in an aqueous solution at room temperature (**Figure S2**), allowing for cell encapsulation under ambient conditions. Physically crosslinked microgels dissociate rapidly at 37 °C and thus require rapid curing.

The gelatin/GelMA microgels are cured to form a bulk hydrogel by photopolymerization in the presence of photoinitiator (PI) and the addition of mTG. Rapid curing of the gelatin/GelMA microgels and the stability of the resulting bulk hydrogel were tested by thermal challenge in a water bath (45 °C) after 2.5 min of crosslinking at room temperature (**Figure 3a-d**). Immersion in a warm water bath removes the physical crosslinks formed by gelatin chains, so a bulk hydrogel would remain intact only if held together through sufficient covalent crosslinks. Experiments were performed using either high PI concentration (0.5%) or low PI concentration (0.05%). PI-induced radicals during photopolymerization are known to be cytotoxic, 35,36 thus minimizing the PI concentration is important for applications in biological systems.

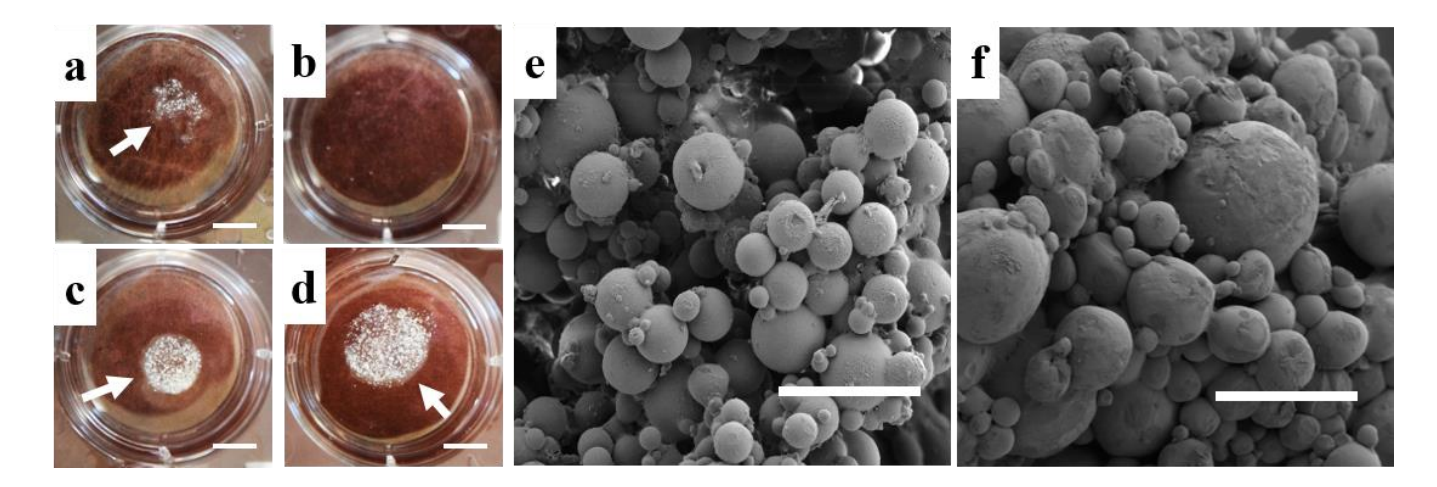


**Figure 3**. Dual-crosslinking approach promotes rapid gelation. Stability of the microgel assembly after curing the microgels only with UV irradiation using (a) 0.5% PI and (b) 0.05% PI, or mTG + UV irradiation using (c) 0.5% PI and (d) 0.05% PI. Scale bar = 5 mm. Arrows indicate the bulk hydrogels. (e-f) SEM images of microgels crosslinked by mTG and UV irradiation using (e) 0.5% PI and (f) 0.05% PI. Scale bar =  $200 \mu m$ .

Microgels cured only by mTG dissociated completely after immersion in 45 °C water bath, indicating that the mTG-based crosslinking was not fast enough to cure the microgels in 2.5 min. When the same microgels were cured by UV irradiation for 2.5 min, a stable bulk hydrogel was formed (Figure 3a) in the presence of high PI concentration (0.5%), due to the rapid formation of covalent crosslinks within and between microgels by photopolymerization among GelMA chains. However, the microgel assembly completely dissociated when cured in the presence of low PI concentration (Figure 3b) because photopolymerization alone was insufficient to cure the microgels. For both PI concentrations, a more stable hydrogel was formed when microgels were cured by both mTG and UV irradiation (Figure 3c, d). The additive effects of UV photopolymerization and mTG facilitates rapid curing of the gelatin/GelMA microgels even with a low PI concentration. When viewed by SEM (Figure 3e, f), hydrogels were clearly made of microspheres, with pores created by the interstitial space.

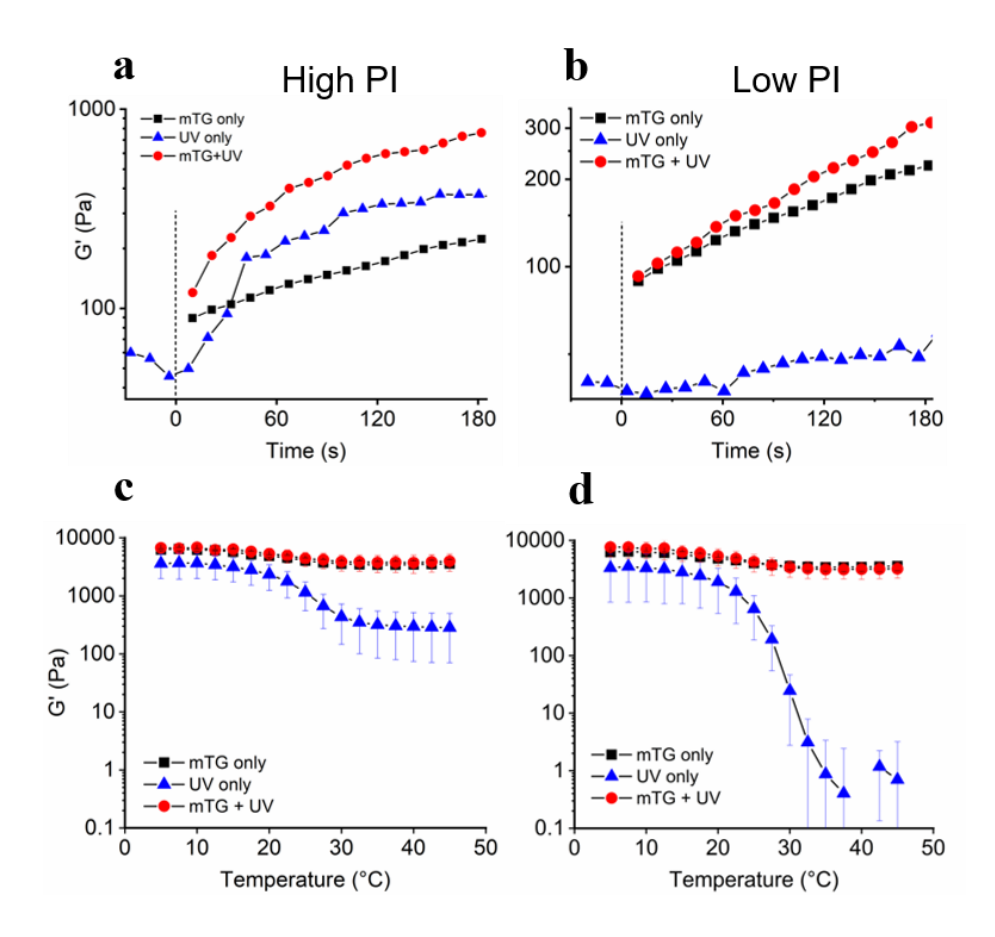


**Figure 4**. Rheological analysis of microporous hydrogel crosslinking. (a, b) Gelation kinetics measured by time sweep of storage moduli (G') for (a) high PI concentration (0.5%) and (b) low PI concentration (0.05%). The dotted lines indicate the time at which UV irradiation began (for 2.5 min). Note that for mTG-only and mTG + UV crosslinking, the crosslinking began as soon as mTG was mixed with microgels, and the moduli before mixing could not be measured. (c, d) Temperature sweep of hydrogels after curing using high PI concentration (c) and low PI concentration (d). For the simplicity of the data presentation, only the storage moduli (G') are presented in this figure. The plots of loss moduli, and frequency sweep can be found in Figure S3. The shown curves are representative of 3 independent experiments.

Gelation kinetics and viscoelastic properties of the hydrogels were quantified by rheology (**Figure 4, Figure S3**). UV irradiation for 2.5 min with a high PI concentration (0.5%) rapidly increased the storage modulus (G') (Figure 4a), compared to the mTG-only crosslinking until removal of the UV source. The combination of both curing methods (mTG + UV) resulted in a rapid initial increase of G' due to photocrosslinking, and a continual increase of G' due to the action of mTG. When a low PI concentration (0.05%) was used (Figure 4b), UV irradiation alone did not result in a significant increase in G', which is consistent with the macroscopic observation (Figure 3b). When both curing methods were combined (mTG + UV), the microgels were cured at a more rapid rate than by mTG alone, demonstrating that the

efficiency of photocrosslinking is improved when used in conjunction with mTG. Temperature sweep after the completion of curing provides further information about the nature of crosslinks within hydrogels.<sup>37</sup> For both PI concentrations, G' decreased for all curing methods as temperature increased, which is characteristic of physically crosslinked gelatin hydrogels (Figure 4c, d). For the case of mTG + UV, G' settled at 3500~4000 Pa above 30 °C, which verifies the presence of covalent crosslinks within the hydrogels which do not dissociate at or above physiological temperature. When the microgels were cured by UV irradiation only, G' settled at much lower values. A higher PI concentration resulted in higher G' at 45 °C (284 +/- 214 Pa vs 0.70 +/- 2.5 Pa for the low PI concentration), indicating increased crosslinking as the PI concentration increased. Theoretically, the stiffness of the bulk hydrogel can be tuned by controlling the stiffness of the microgels either by changing the crosslinking density or by incorporating various nanomaterials.<sup>38</sup>

In addition to rapid curing, adhesion of the resulting hydrogel to the applied tissue serves to improve clinical viability of the injectable formulation,<sup>39–41</sup> by improving the hydrogel retention at the intended target site.<sup>42</sup> Previously, we demonstrated that the microporous hydrogel made by assembly of gelatin microgels adhered to porcine corneal tissue within 1 hour by the action of mTG.<sup>31</sup> mTG has been used as a tissue adhesive and is considered biocompatible.<sup>43,44</sup> Porcine cornea was used as a model tissue for simple visualization. mTG-catalyzed tissue adhesion was examined when used in conjunction with photopolymerization (**Figure 5**). The microgels were injected into an 8 mm hole in a porcine cornea and allowed to crosslink by UV irradiation alone or by both mTG crosslinking and UV irradiation (mTG + UV). After curing, the cornea-hydrogel construct underwent thermal challenge in a water bath (45 °C).

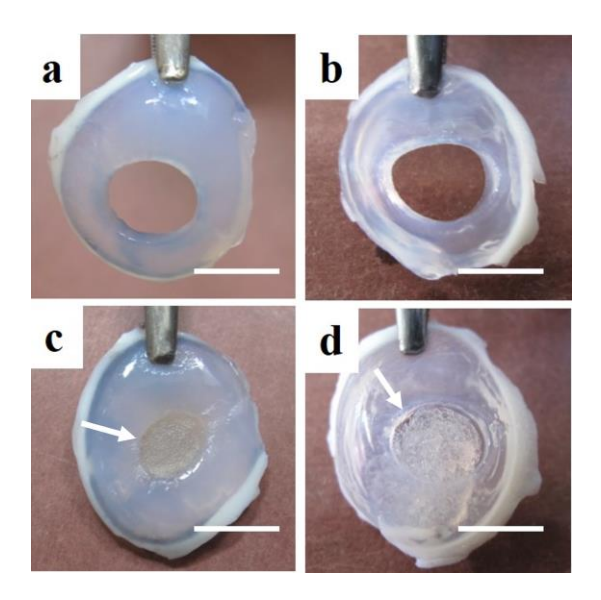


**Figure 5**. Tissue adhesion test. Microgels were injected into 8 mm holes made in porcine cornea and crosslinked for 2.5 min by UV irradiation only using (a) 0.5% PI, and (b) 0.05% PI, or by mTG + UV irradiation using (c) 0.5% PI and (d) 0.05% PI. Scale bar = 10 mm. Hydrogels are denoted by arrows.

For the high PI concentration, UV irradiation created a stable hydrogel, but it readily detached from the tissue when immersed in the warm water bath (Figure 5a). When the low PI concentration was used, the UV irradiation alone did not form a bulk hydrogel, precluding tissue adhesion (Figure 5b). When mTG was added in addition to UV irradiation, not only did a stable hydrogel form (Figure 3c, d), but the resulting hydrogel also adhered to the cornea tissue with both PI concentrations (Figure 5c, d). These results clearly show that the dual-crosslinking achieves rapid curing of the gelatin/GelMA microgels and enables stable adhesion of the hydrogel to tissue even at low PI concentration (0.05%). Stable tissue adhesion of gelatin-based hydrogels by mTG is consistent with our previous results.<sup>44</sup> Our results also show that photopolymerization alone does not allow the tissue adhesion of the microgel-based hydrogel even at a high PI concentration (0.5%).

Two independent factors contribute to stable adhesion of a hydrogel to a wet tissue surface – interfacial adhesion (i.e. crosslinking between the hydrogel and tissue) and cohesion (i.e. mechanical strength of the hydrogel). We attribute the rapid and stable tissue adhesion of the microgel-based hydrogel to the simultaneous enhancement of both interfacial adhesion (by mTG) and cohesion (by UV) enabled by the dual-crosslinking approach.

Enzymatic degradation of gelatin/GelMA microgels and the annealed hydrogel was measured using collagenase type II (**Figure S4**) as previously described.<sup>45</sup> Both microgels and the bulk hydrogel degraded completely within 24 hours, demonstrating the biodegradability of this formulation. This result is consistent with the fact that gelatin and GelMA have been shown to be degraded both *in vitro* and *in vivo* by various enzymes.<sup>31,46</sup>

In situ cell encapsulation in a hydrogel is an important technology for the delivery of viable cells for wound healing and regenerative medicine. <sup>26,47,48</sup> The feasibility of using the microgel-based injectable hydrogel for cell delivery was investigated using human dermal fibroblasts (hDFs) (**Figure 6**, **Figure S5**-6). Unlike most injectable hydrogel systems in which cells are homogeneously distributed within the hydrogel, cells are encapsulated in the interstitial space between microgels.

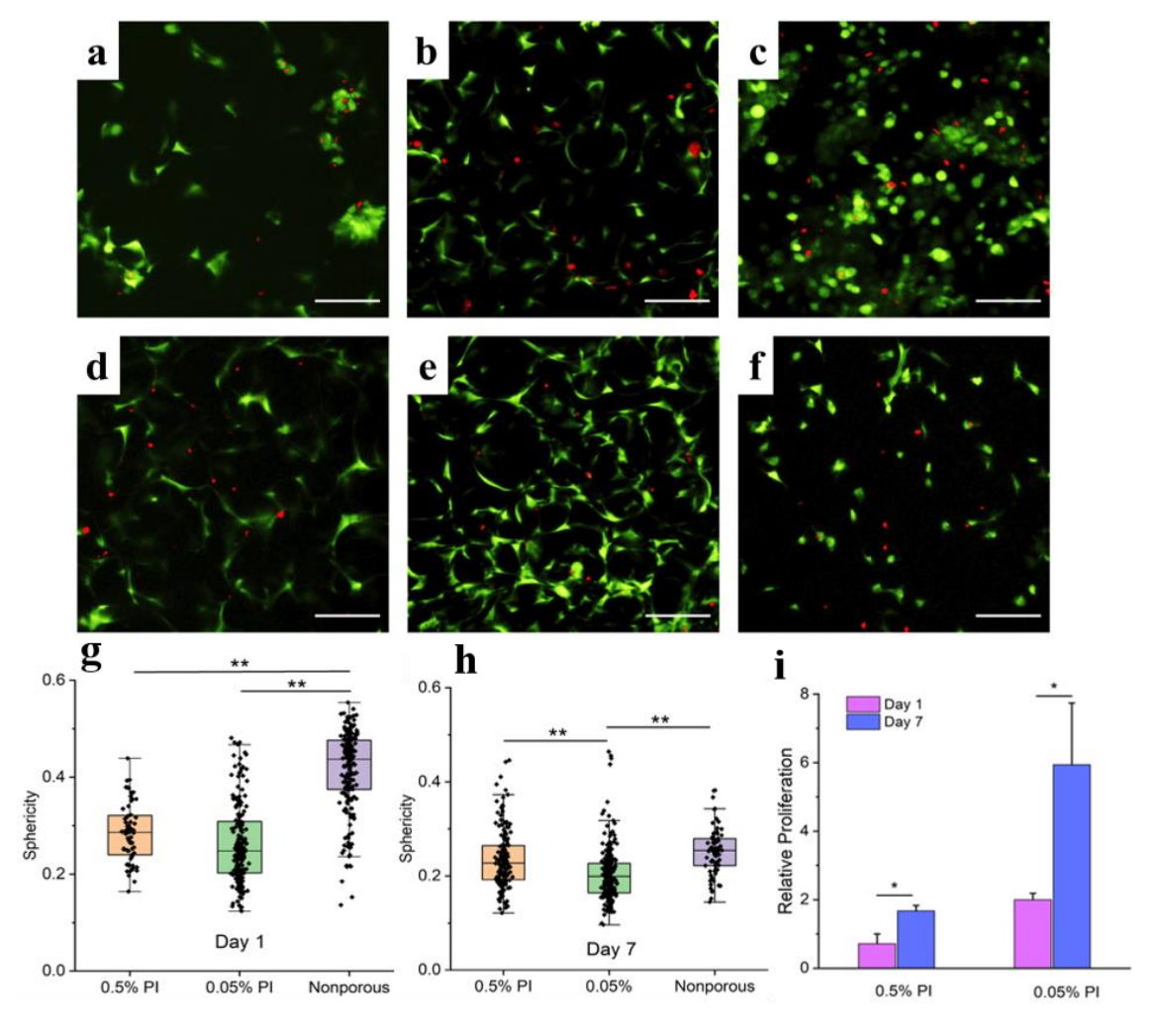


**Figure 6**. Cell encapsulation in the interstitial space between annealed microgels. (a-f) 2D projections of confocal microscope images of live/dead assay. (a-c) Day 1 and (d-f) day 7 post-encapsulation. The microgels were cured with mTG and UV irradiation using (a, d) 0.5% or (b, e) 0.05% PI concentration. Nonporous hydrogel was formed with mTG and UV irradiation using 0.05% PI concentration. Scale bar

= 100  $\mu$ m, green = living, red = dead. (g-h) Sphericity of encapsulated cells (g) day 1 and (h) day 7 post encapsulation. (i) Cell proliferation in the microporous hydrogels relative to the nonporous control (n=3). (\*) = p < 0.05 and (\*\*) = p < 0.001

Cell-encapsulating constructs were formed by curing the microgels by both mTG and UV irradiation using either 0.5% PI or 0.05% PI. For a comparison, cells were also encapsulated in a nonporous hydrogel, which was formed by crosslinking a homogeneous solution of gelatin and GelMA using mTG and UV irradiation (with 0.05% PI). At all time points (day 1 and day 7 post encapsulation), cell viability was high for all groups (Figure 6a-f, Figure S6a), although the porous hydrogel with 0.5% PI resulted in the lowest viability on day 1 (p > 0.05). Strikingly, the cells encapsulated in the microporous hydrogels exhibited fully spread morphologies as early as day 1 post encapsulation (Figure 6a-b, g). Rapid spreading of encapsulated cells, which is attributed to the large available void space within the porous hydrogels, is distinct from most nonporous hydrogels in which the encapsulated cells are trapped by the polymer chains and cannot spread immediately (Figure 6c). Although it is not the focus of this report, the current injectable formulation, which induces rapid spreading of the encapsulated cells, will be useful when the differentiation into a specific lineage is facilitated by cell spreading (e.g. osteogenic differentiation of MSCs).<sup>49</sup>

The advantage of encapsulating cells in the pores of the microgel-assembly was further proven by the live/dead assay performed on day 7 post encapsulation (Figure 6d-f). As on day 1, the cells were well-spread around the microgels within the interstitial space, resulting in decreased sphericities compared to day 1 (Figure 6h). The cells encapsulated in the nonporous hydrogel still exhibited higher sphericity likely due to prevention of spreading by the polymer mesh. The detailed structures of actin cytoskeleton on day 7 confirmed these results (**Figure S7**).

The benefit of lowering the PI concentration is highlighted by the assessment of cell proliferation. At both time points, the samples with 0.05% PI concentration resulted in higher proliferation than the samples with 0.5% PI concentration (Figure 6i), presumably due to decreased exposure of cells to free radicals during encapsulation. This result is supported by the significant increase in cytotoxicity on day 1

for the 0.5% PI group measured by lactate dehydrogenase (LDH) release (Figure S6b). By day 7, LDH release was substantially lower for both groups, indicating that the lower proliferation of the 0.5% PI group resulted from the initial cytotoxicity during the photopolymerization. For both PI concentrations, proliferation on day 7 was higher than the cells encapsulated in the nonporous hydrogels, which is consistent with the recent report that MSCs encapsulated in a microporous hydrogel exhibited significantly higher proliferation than the cells encapsulated in nonporous hydrogel in vivo. <sup>26</sup>

Next, hMSC encapsulation was performed to demonstrate high hMSC viability in this fast-curing microporous hydrogel and its potential use in MSC-based therapies, such as immunomodulation (**Figure 7**). MSC delivery has been explored to reduce autoimmune responses to organ transplants or biomaterial implants, <sup>50,51</sup> and treat chronic inflammatory diseases, <sup>52</sup> whereby MSCs are primed by pro-inflammatory signals, such as IFN-γ before delivery to improve their immunosuppressive properties. <sup>53</sup> A major limiting factor of MSC-based therapy is the limited residence time of MSCs at the site of injection, and thus encapsulation in biomaterials is being explored to address this limitation. <sup>54,55</sup> The microporous hydrogel platform described here is advantageous for this application due to having high internal surface area and the ability to promote cell growth.

Similar to the encapsulated hDFs, hMSCs rapidly spread around the microgels as early as day 1 (**Figure S8**), and showed improved cell spreading and proliferation over 7 days in comparison to the nonporous counterpart (Figure 7a-d).

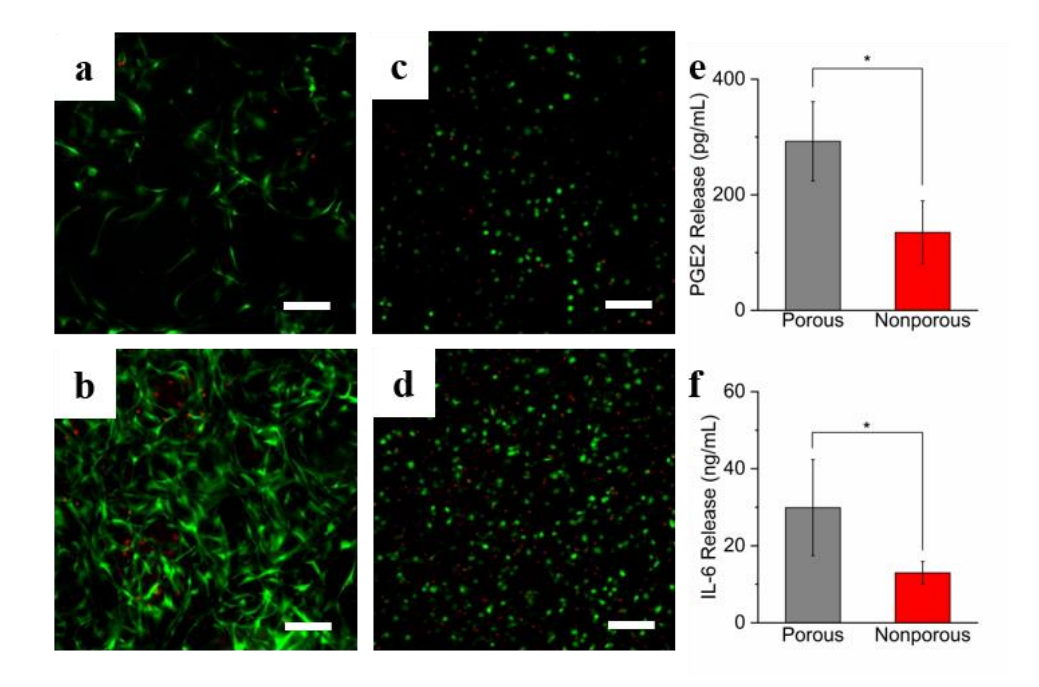


**Figure 7**. Gelatin/GelMA composite microgels enhance hMSC growth and promote secretion of anti-inflammatory cytokines. (a-d) 2D projections of confocal microscopy images for cells encapsulated in the (a, b) microporous and (c, d) nonporous hydrogels. Images were taken on (a, c) day 1 and (b, d) day 7. (e, f) Scale bar: 100 μm. (e, f) Secretion of (e) prostaglandin E2 and (f) interleukin-6 after encapsulation of MSCs primed by IFN-γ.

When hMSCs were primed with IFN-γ (50 ng/mL) for 24 hours immediately prior to encapsulation, the secretion of factors involved in MSC-mediated immunosuppression (PGE2, IL-6)<sup>56</sup> was improved by encapsulation in the microporous hydrogel (Figure 7e, f). These results show that this injectable microporous hydrogel can be used to deliver hMSCs with high viability and alleviate local inflammation by the release of anti-inflammatory factors when the hMSCs are primed by IFN-γ. This study provides context and demonstrates the potential to deliver MSCs via microporous hydrogel as an anti-inflammatory treatment.

#### CONCLUSIONS

Overall, the injectable hydrogel formulation described here has several major advantages compared to previously reported injectable hydrogels: (1) enhanced thermal stability of microgels allows for more favorable conditions during cell encapsulation than GelMA-only microgels; (2) rapid gelation (2.5 min) under UV irradiation even at a low PI concentration (0.05%) was achieved due to the synergistic

actions of UV photopolymerization and mTG-based enzymatic crosslinking; (3) the use of low PI concentration results in high viability, proliferation and low cytotoxicity of the encapsulated cells; (4) due to the action of mTG in conjunction with UV photopolymerization, the hydrogel can adhere to the target tissue stably within 2.5 min; (5) the presence of pores allows rapid adhesion, spreading, and proliferation of the encapsulated cells. We demonstrated the applicability of this platform for priming MSCs for immunomodulation, and we anticipate that this formulation will find many applications related to cell delivery-based therapeutics.

# FIGURES

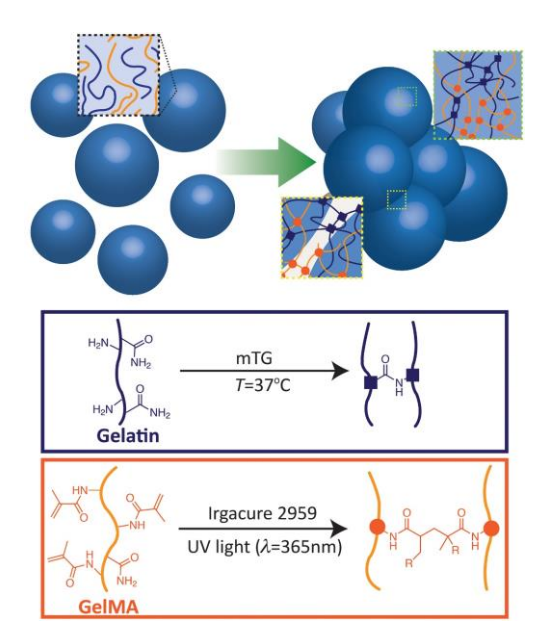


**Figure 1**. Schematic of the dual-crosslinking mechanisms of gelatin/GelMA microgels used to form a bulk hydrogel. A dual crosslinking approach is employed to rapidly cure microgels.

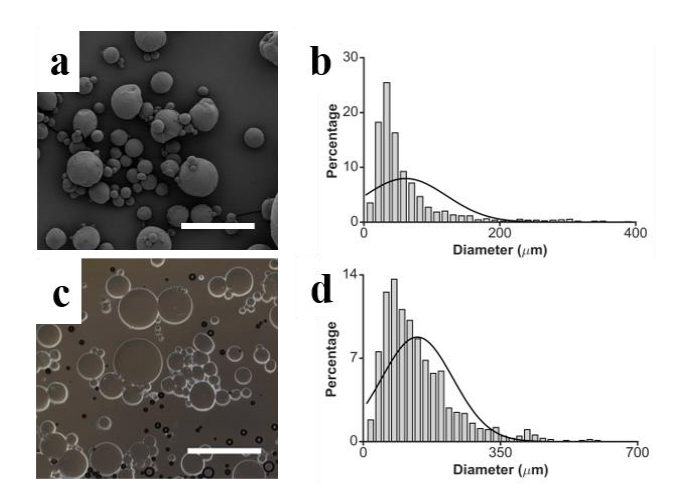


Figure 2. Composite microgel characterization. (a) SEM image of dry gelatin/GelMA microspheres. Scale bar = 200  $\mu$ m (b) Size distribution of dry microspheres. The average diameter = 61  $\pm$  60  $\mu$ m. (c) Optical micrograph of gelatin/GelMA microgels in PBS. Scale bar = 200  $\mu$ m. (d) Size distribution of swelled microgels. The average diameter = 139  $\pm$  90  $\mu$ m.

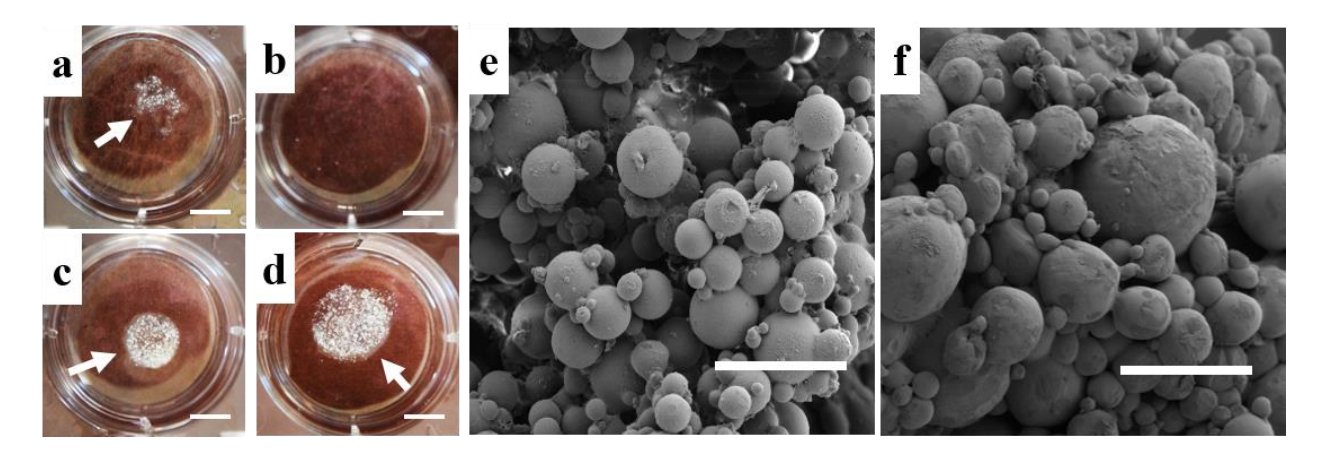
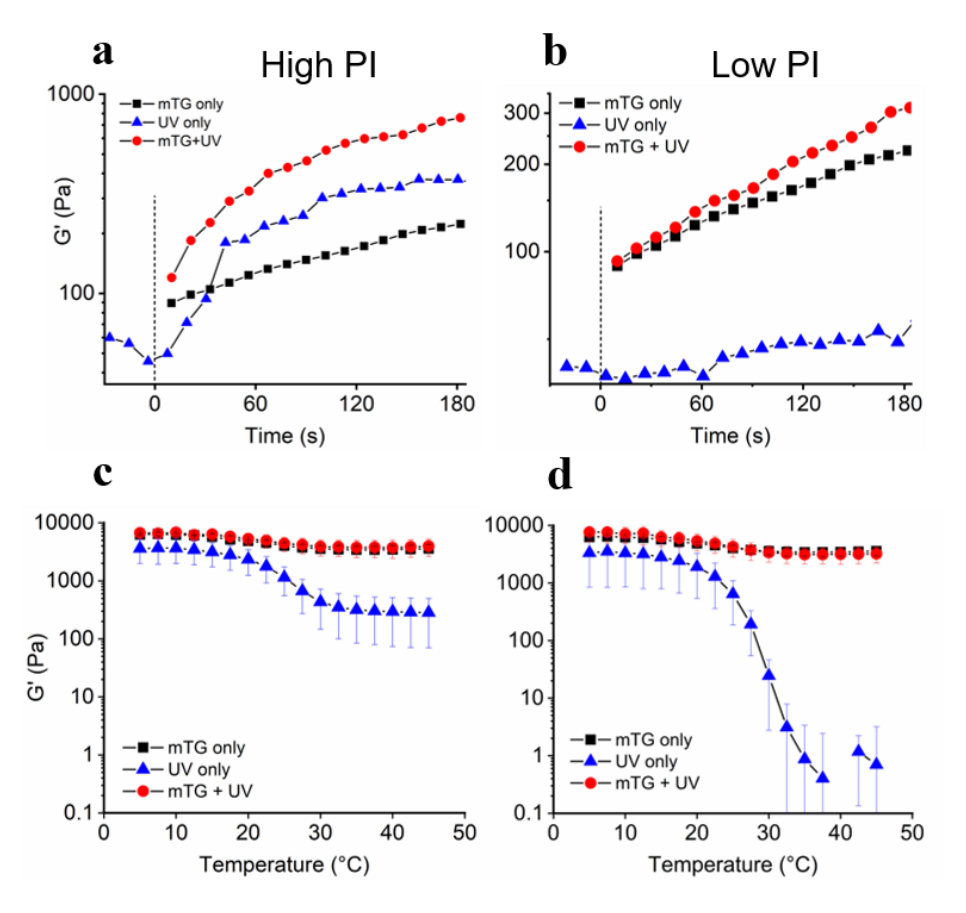
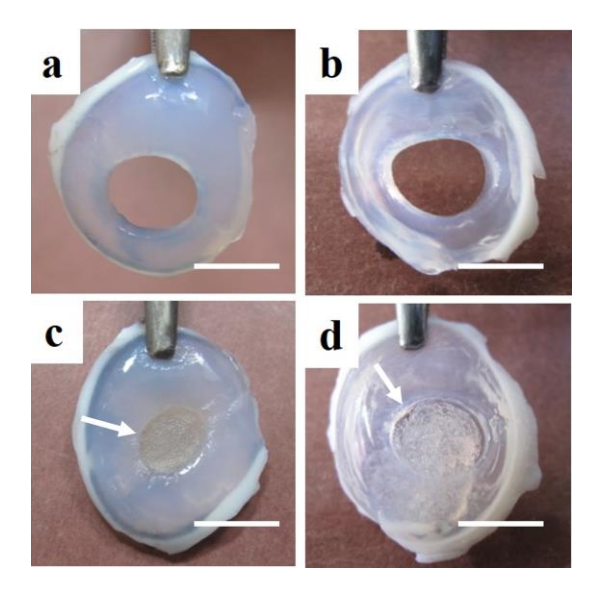


Figure 3. Dual-crosslinking approach promotes rapid gelation. Stability of the microgel assembly after curing the microgels only with UV irradiation using (a) 0.5% PI and (b) 0.05% PI, or mTG + UV irradiation using (c) 0.5% PI and (d) 0.05% PI. Scale bar = 5 mm. Arrows indicate the bulk hydrogels. (e-f) SEM images of microgels crosslinked by mTG and UV irradiation using (e) 0.5% PI and (f) 0.05% PI. Scale bar =  $200~\mu m$ .



**Figure 4**. Rheological analysis of microporous hydrogel crosslinking. (a, b) Gelation kinetics measured by time sweep of storage moduli (G') for (a) high PI concentration (0.5%) and (b) low PI concentration (0.05%). The dotted lines indicate the time at which UV irradiation began (for 2.5 min). Note that for mTG-only and mTG + UV crosslinking, the crosslinking began as soon as mTG was mixed with microgels, and the moduli before mixing could not be measured. (c, d) Temperature sweep of hydrogels after curing using high PI concentration (c) and low PI concentration (d). For the simplicity of the data presentation, only the storage moduli (G') are presented in this figure. The plots of loss moduli, and frequency sweep can be found in Figure S3. The shown curves are representative of 3 independent experiments.



**Figure 5**. Tissue adhesion test. Microgels were injected into 8 mm holes made in porcine cornea and crosslinked for 2.5 min by UV irradiation only using (a) 0.5% PI, and (b) 0.05% PI, or by mTG + UV irradiation using (c) 0.5% PI and (d) 0.05% PI. Scale bar = 10 mm. Hydrogels are denoted by arrows.

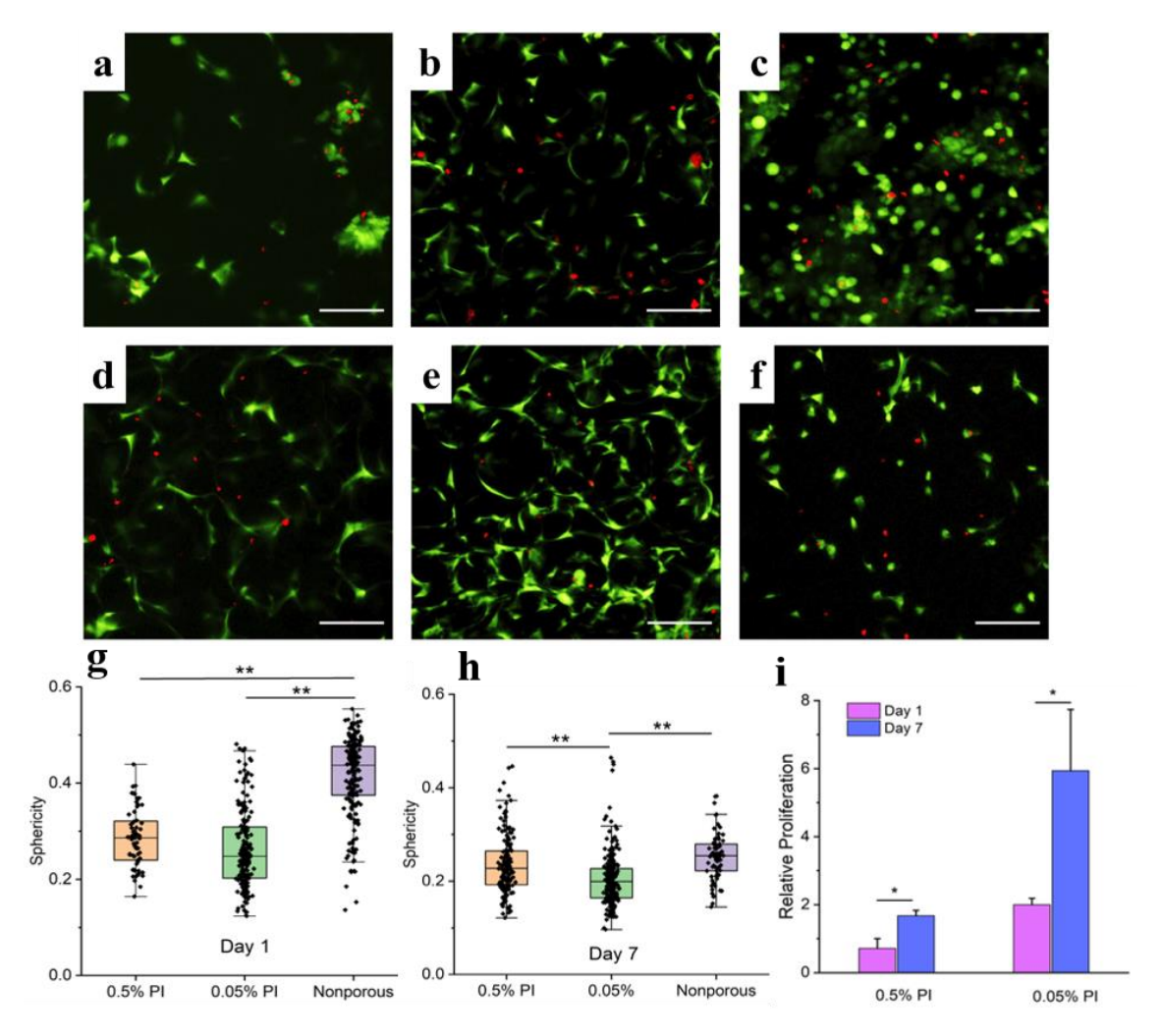


**Figure 6**. Cell encapsulation in the interstitial space between annealed microgels. (a-f) 2D projections of confocal microscope images of live/dead assay. (a-c) Day 1 and (d-f) day 7 postencapsulation. The microgels were cured with mTG and UV irradiation using (a, d) 0.5% or (b, e) 0.05% PI concentration. Nonporous hydrogel was formed with mTG and UV irradiation using 0.05% PI concentration. Scale bar = 100  $\mu$ m, green = living, red = dead. (g-h) Sphericity of encapsulated cells (g) day 1 and (h) day 7 post encapsulation. (i) Cell proliferation in the microporous hydrogels relative to the nonporous control (n=3). (\*) = p < 0.05 and (\*\*) = p < 0.001

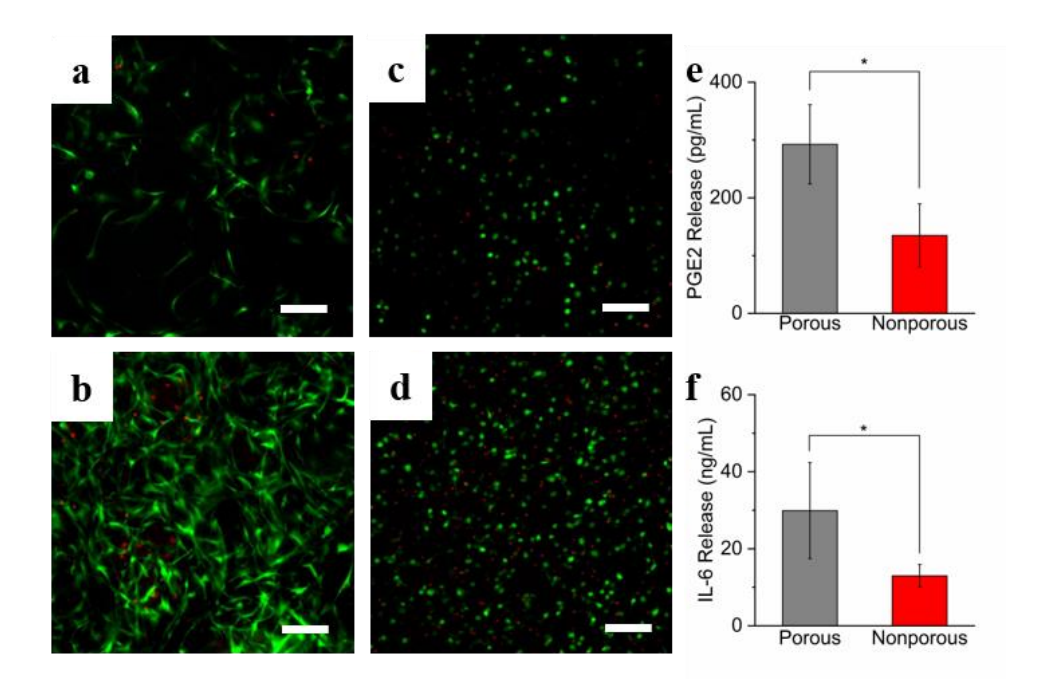


Figure 7. Gelatin/GelMA composite microgels enhance hMSC growth and promote secretion of anti-inflammatory cytokines. (a-d) 2D projections of confocal microscopy images for cells encapsulated in the (a, b) microporous and (c, d) nonporous hydrogels. Images were taken on (a, c) day 1 and (b, d) day 7. (e, f) Scale bar: 100 μm. (e, f) Secretion of (e) prostaglandin E2 and (f) interleukin-6 after encapsulation of MSCs primed by IFN-γ.

ASSOCIATED CONTENT

**Supporting Information** 

The following files are available free of charge.

Supplementary live/dead confocal images (Figure S1); gel stability under ambient conditions

(Figure S2); comprehensive rheology information (Figure S3); gel degradation assay (Figure S4);

compiled 3D confocal images (Figure S5); cell viability and cytotoxicity assay results (Figure S6);

Actin and nuclei staining of encapsulated hDFs (Figure S7); High magnification confocal image

of hMSCs surrounding a microgel (Figure S8) (PDF)

**AUTHOR INFORMATION** 

**Corresponding Author** 

\* Email: KyungJae.Jeong@unh.edu

ORCID number

Kyung Jae Jeong: 0000-0002-8749-9830

**Notes** 

The authors have no conflicts of interest to declare.

**ACKNOWLEDGMENT** 

The authors would like to thank NIH COBRE Center of Integrated Biomedical and

Bioengineering Research (CIBBR, P20 GM113131) through an Institutional Development Award

(IDeA) from the National Institute of General Medical Sciences, National Eye Institute of the

26

National Institutes of Health under award number 1R21EY02795301 and National Science Foundation under award number OIA-1757371 for supporting this research.

### **ABBREVIATIONS**

hDF, human dermal fibroblast; PI, photoinitiator; GelMA, gelatin methacryloyl; mTG, microbial transglutaminase; SEM, scanning electron microscopy; G', storage modulus; hMSC, human mesenchymal stem cell; LDH, lactate dehydrogenase; IFN-γ, interferon-γ; PGE2, prostaglandin E2; IL-6, interleukin-6.

#### REFERENCES

- (1) Li, Y.; Rodrigues, J.; Tomás, H. Injectable and Biodegradable Hydrogels: Gelation, Biodegradation and Biomedical Applications. *Chem. Soc. Rev.* **2012**, *41*, 2193–2221. DOI: 10.1039/c1cs15203c
- (2) Liu, M.; Zeng, X.; Ma, C.; Yi, H.; Ali, Z.; Mou, X.; Li, S.; Deng, Y.; He, N. Injectable Hydrogels for Cartilage and Bone Tissue Engineering. *Bone Res.* **2017**, *5*, 17014 DOI: 10.1038/boneres.2017.14
- (3) Ren, K.; He, C.; Xiao, C.; Li, G.; Chen, X. Injectable Glycopolypeptide Hydrogels as Biomimetic Scaffolds for Cartilage Tissue Engineering. *Biomaterials* **2015**, *51*, 238–249. DOI: 10.1016/j.biomaterials.2015.02.026
- (4) Popa, E. G.; Caridade, S. G.; Mano, J. F.; Reis, R. L.; Gomes, M. E. Chondrogenic Potential of Injectable κ-Carrageenan Hydrogel with Encapsulated Adipose Stem Cells for Cartilage Tissue-Engineering Applications. *J. Tissue Eng. Regen. Med.* **2015**, *9*, 550–563. DOI: 10.1002/term.1683
- (5) Jooybar, E.; Abdekhodaie, M. J.; Alvi, M.; Mousavi, A.; Karperien, M.; Dijkstra, P. J. An Injectable Platelet Lysate-Hyaluronic Acid Hydrogel Supports Cellular Activities and Induces Chondrogenesis of Encapsulated Mesenchymal Stem Cells. *Acta Biomater.* **2019**, *83*, 233–244. DOI: 10.1016/j.actbio.2018.10.031
- (6) Cai, L.; Dewi, R. E.; Heilshorn, S. C. Injectable Hydrogels with In Situ Double Network Formation Enhance Retention of Transplanted Stem Cells. *Adv. Funct. Mater.* **2015**, *25*, 1344–1351. DOI: 10.1002/adfm.201403631

- (7) Anjum, F.; Lienemann, P. S.; Metzger, S.; Biernaskie, J.; Kallos, M. S.; Ehrbar, M. Enzyme Responsive GAG-Based Natural-Synthetic Hybrid Hydrogel for Tunable Growth Factor Delivery and Stem Cell Differentiation. *Biomaterials* **2016**, *87*, 104–117. DOI: 10.1016/j.biomaterials.2016.01.050
- (8) Lindsey, S.; Piatt, J. H.; Worthington, P.; Sönmez, C.; Satheye, S.; Schneider, J. P.; Pochan, D. J.; Langhans, S. A. Beta Hairpin Peptide Hydrogels as an Injectable Solid Vehicle for Neurotrophic Growth Factor Delivery. *Biomacromolecules* **2015**, *16*, 2672–2683. DOI 10.1021/acs.biomac.5b00541
- (9) Park, H.; Temenoff, J. S.; Tabata, Y.; Caplan, A. I.; Mikos, A. G. Injectable Biodegradable Hydrogel Composites for Rabbit Marrow Mesenchymal Stem Cell and Growth Factor Delivery for Cartilage Tissue Engineering. *Biomaterials* **2007**, *28*, 3217–3227. DOI: 10.1016/j.biomaterials.2007.03.030
- (10) Sun, J. E. P.; Stewart, B.; Litan, A.; Lee, S. J.; Schneider, J. P.; Langhans, S. A.; Pochan, D. J. Sustained Release of Active Chemotherapeutics from Injectable-Solid β-Hairpin Peptide Hydrogel. *Biomater. Sci.* **2016**, *4*, 839–848. DOI: 10.1039/c5bm00538h
- (11) Norouzi, M.; Nazari, B.; Miller, D. W. Injectable Hydrogel-Based Drug Delivery Systems for Local Cancer Therapy. *Drug Discovery Today* **2016**, *21*, 1835–1849. DOI: 10.1016/j.drudis.2016.07.006
- (12) Joshi, N.; Yan, J.; Levy, S.; Bhagchandani, S.; Slaughter, K. V.; Sherman, N. E.; Amirault, J.; Wang, Y.; Riegel, L.; He, X.; Rui, T. S.; Valic, M.; Vemula, P. K.; Miranda, O. R.; Levy, O.; Gravallese, E. M.; Aliprantis, A. O.; Ermann, J.; Karp, J. M. Towards an Arthritis Flare-

- Responsive Drug Delivery System. *Nat. Commun.* **2018**, *9* 1275. DOI: 10.1038/s41467-018-03691-1
- (13) Li, L.; Lu, C.; Wang, L.; Chen, M.; White, J.; Hao, X.; McLean, K. M.; Chen, H.; Hughes, T. C. Gelatin-Based Photocurable Hydrogels for Corneal Wound Repair. *ACS Appl. Mater. Interfaces* **2018**, *10*, 13283–13292. DOI: 10.1021/acsami.7b17054
- (14) Phelps, E. A.; Enemchukwu, N. O.; Fiore, V. F.; Sy, J. C.; Murthy, N.; Sulchek, T. A.; Barker, T. H.; García, A. J. Maleimide Cross-Linked Bioactive PEG Hydrogel Exhibits Improved Reaction Kinetics and Cross-Linking for Cell Encapsulation and in Situ Delivery. *Adv. Mater.* **2012**, *24*, 64–70. DOI: 10.1002/adma.201103574
- (15) Chen, M. B.; Srigunapalan, S.; Wheeler, A. R.; Simmons, C. A. A 3D Microfluidic Platform Incorporating Methacrylated Gelatin Hydrogels to Study Physiological Cardiovascular Cell-Cell Interactions. *Lab Chip* **2013**, *13*, 2591–2598. DOI: 10.1039/c3lc00051f
- (16) Griffin, D. R.; Weaver, W. M.; Scumpia, P. O.; Di Carlo, D.; Segura, T. Accelerated Wound Healing by Injectable Microporous Gel Scaffolds Assembled from Annealed Building Blocks. *Nat. Mater.* **2015**, *14*, 737–744. DOI: 10.1038/nmat4294
- (17) Sheikhi, A.; de Rutte, J.; Haghniaz, R.; Akouissi, O.; Sohrabi, A.; Di Carlo, D.; Khademhosseini, A. Microfluidic-Enabled Bottom-up Hydrogels from Annealable Naturally-Derived Protein Microbeads. *Biomaterials* **2019**, *192*, 560–568. DOI: 10.1016/j.biomaterials.2018.10.040

- (18) Sideris, E.; Griffin, D. R.; Ding, Y.; Li, S.; Weaver, W. M.; Di Carlo, D.; Hsiai, T.; Segura, T. Particle Hydrogels Based on Hyaluronic Acid Building Blocks. *ACS Biomater. Sci. Eng.* **2016**, *2*, 2034–2041. DOI: 10.1021/acsbiomaterials.6b00444
- (19) Darling, N. J.; Sideris, E.; Hamada, N.; Carmichael, S. T.; Segura, T. Injectable and Spatially Patterned Microporous Annealed Particle (MAP) Hydrogels for Tissue Repair Applications. *Adv. Sci.* **2018**, *5*, 1801046. DOI: 10.1002/advs.201801046
- (20) Daly, A. C.; Riley, L.; Segura, T.; Burdick, J. A. Hydrogel Microparticles for Biomedical Applications. *Nat. Rev. Mater.* **2020**, *5*, 20-43 DOI: 10.1038/s41578-019-0148-6
- (21) Mealy, J. E.; Chung, J. J.; Jeong, H. H.; Issadore, D.; Lee, D.; Atluri, P.; Burdick, J. A. Injectable Granular Hydrogels with Multifunctional Properties for Biomedical Applications. *Adv. Mater.* **2018**, *30* 1705912. DOI: 10.1002/adma.201705912
- (22) Arun Kumar, R.; Sivashanmugam, A.; Deepthi, S.; Iseki, S.; Chennazhi, K. P.; Nair, S. V.; Jayakumar, R. Injectable Chitin-Poly(ε-Caprolactone)/Nanohydroxyapatite Composite Microgels Prepared by Simple Regeneration Technique for Bone Tissue Engineering. *ACS Appl. Mater. Interfaces* **2015**, *7*, 9399–9409. DOI: 10.1021/acsami.5b02685
- (23) Xin, S.; Chimene, D.; Garza, J. E.; Gaharwar, A. K.; Alge, D. L. Clickable PEG Hydrogel Microspheres as Building Blocks for 3D Bioprinting. *Biomater. Sci.* **2019**, *7*, 1179–1187. DOI: 10.1039/c8bm01286e
- (24) Qu, J.; Zhao, X.; Liang, Y.; Zhang, T.; Ma, P. X.; Guo, B. Antibacterial Adhesive Injectable Hydrogels with Rapid Self-Healing, Extensibility and Compressibility as Wound Dressing for

- Joints Skin Wound Healing. *Biomaterials* **2018**, *183*, 185–199. DOI: 10.1016/j.biomaterials.2018.08.044
- (25) Huang, W.; Li, X.; Shi, X.; Lai, C. Microsphere Based Scaffolds for Bone Regenerative Applications. *Biomater. Sci.* **2014**, *2*, 1145–1153. DOI: 10.1039/c4bm00161c
- (26) Koh, J.; Griffin, D. R.; Archang, M. M.; Feng, A.; Horn, T.; Margolis, M.; Zalazar, D.; Segura, T.; Scumpia, P. O.; Di Carlo, D. Enhanced In Vivo Delivery of Stem Cells Using Microporous Annealed Particle Scaffolds. *Small* **2019**, *15*, 1903147. DOI: 10.1002/smll.201903147
- (27) Duan, B.; Shou, K.; Su, X.; Niu, Y.; Zheng, G.; Huang, Y.; Yu, A.; Zhang, Y.; Xia, H.; Zhang, L. Hierarchical Microspheres Constructed from Chitin Nanofibers Penetrated Hydroxyapatite Crystals for Bone Regeneration. *Biomacromolecules* **2017**, *18*, 2080–2089. DOI: 10.1021/acs.biomac.7b00408
- (28) Jiang, W.; Li, M.; Chen, Z.; Leong, K. W. Cell-Laden Microfluidic Microgels for Tissue Regeneration. *Lab Chip* **2016**, *16*, 4482–4506. DOI: 10.1039/c6lc01193d
- (29) Xin, S.; Wyman, O. M.; Alge, D. L. Assembly of PEG Microgels into Porous Cell-Instructive 3D Scaffolds via Thiol-Ene Click Chemistry. *Adv. Healthc. Mater.* **2018**, *7*, 1800160. DOI: 10.1002/adhm.201800160
- (30) Choi, Y. H.; Kim, S. H.; Kim, I. S.; Kim, K. M.; Kwon, S. K.; Hwang, N. S. Gelatin-Based Micro-Hydrogel Carrying Genetically Engineered Human Endothelial Cells for Neovascularization. *Acta Biomater.* **2019**, *95*, 285-296. DOI: 10.1016/j.actbio.2019.01.057

- (31) Hou, S.; Lake, R.; Park, S.; Edwards, S.; Jones, C.; Jeong, K. J. Injectable Macroporous Hydrogel Formed by Enzymatic Cross-Linking of Gelatin Microgels. *ACS Appl. Bio Mater.* **2018**, *1*, 1430-1439. DOI: 10.1021/acsabm.8b00380
- (32) Besser, R. R.; Bowles, A. C.; Alassaf, A.; Carbonero, D.; Claure, I.; Jones, E.; Reda, J.; Wubker, L.; Batchelor, W.; Ziebarth, N.; Silvera, R.; Khan, A.; Maciel, R.; Saporta, M.; Agarwal, A. Enzymatically Crosslinked Gelatin-Laminin Hydrogels for Applications in Neuromuscular Tissue Engineering. *Biomater. Sci.* **2020**, *8*, 591–606. DOI: 10.1039/c9bm01430f
- (33) Sabnis, A.; Rahimi, M.; Chapman, C.; Nguyen, K. T. Cytocompatibility Studies of an in Situ Photopolymerized Thermoresponsive Hydrogel Nanoparticle System Using Human Aortic Smooth Muscle Cells. *J. Biomed. Mater. Res. A* **2009**, *91*, 52–59. DOI: 10.1002/JBM.A.32194.
- (34) Zoratto, N.; Di Lisa, D.; de Rutte, J.; Sakib, M. N.; Alves e Silva, A. R.; Tamayol, A.; Di Carlo, D.; Khademhosseini, A.; Sheikhi, A. In Situ Forming Microporous Gelatin Methacryloyl Hydrogel Scaffolds from Thermostable Microgels for Tissue Engineering. *Bioeng. Transl. Med.* **2020**, *5*. DOI: 10.1002/BTM2.10180.
- (35) Shearier, E. R.; Bowen, P. K.; He, W.; Drelich, A.; Drelich, J.; Goldman, J.; Zhao, F. In Vitro Cytotoxicity, Adhesion, and Proliferation of Human Vascular Cells Exposed to Zinc. *ACS Biomater. Sci. Eng.* **2016**, *2*, 634–642. DOI: 10.1021/acsbiomaterials.6b00035
- (36) Wang, M. O.; Etheridge, J. M.; Thompson, J. A.; Vorwald, C. E.; Dean, D.; Fisher, J. P. Evaluation of the In Vitro Cytotoxicity of Cross-Linked Biomaterials. *Biomacromolecules* **2013**, *14*, 1321–1329. DOI: 10.1021/bm301962f

- (37) Van Den Bulcke, A. I.; Bogdanov, B.; De Rooze, N.; Schacht, E. H.; Cornelissen, M.; Berghmans, H. Structural and Rheological Properties of Methacrylamide Modified Gelatin Hydrogels. **2000**, *1*, 31-38. DOI: 10.1021/bm990017d
- (38) Pan, C.; Liu, L.; Chen, Q.; Zhang, Q.; Guo, G. Tough, Stretchable, Compressive Novel Polymer/Graphene Oxide Nanocomposite Hydrogels with Excellent Self-Healing Performance. *ACS Appl. Mater. Interfaces* **2017**, *9*, 38052–38061. DOI: 10.1021/acsami.7b12932
- (39) Nicodemus, G. D.; Bryant, S. J. Cell Encapsulation in Biodegradable Hydrogels for Tissue Engineering Applications. *Tissue Eng.*, *Part B* **2008**, *14*, 149-165. DOI: 10.1089/ten.teb.2007.0332
- (40) Wang, D. A.; Varghese, S.; Sharma, B.; Strehin, I.; Fermanian, S.; Gorham, J.; Fairbrother, D. H.; Cascio, B.; Elisseeff, J. H. Multifunctional Chondroitin Sulphate for Cartilage Tissue-Biomaterial Integration. *Nat. Mater.* **2007**, *6*, 385–392. DOI: 10.1038/nmat1890
- (41) Seliktar, D. Designing Cell-Compatible Hydrogels for Biomedical Applications. *Science*.2012, 336, 1124–1128. DOI: 10.1126/science.1214804
- (42) Feng, Q.; Wei, K.; Lin, S.; Xu, Z.; Sun, Y.; Shi, P.; Li, G.; Bian, L. Mechanically Resilient, Injectable, and Bioadhesive Supramolecular Gelatin Hydrogels Crosslinked by Weak Host-Guest Interactions Assist Cell Infiltration and in Situ Tissue Regeneration. *Biomaterials* **2016**, *101*, 217–228. DOI: 10.1016/j.biomaterials.2016.05.043
- (43) McDermott, M. K.; Chen, T.; Williams, C. M.; Markley, K. M.; Payne, G. F. Mechanical Properties of Biomimetic Tissue Adhesive Based on the Microbial Transglutaminase-Catalyzed Crosslinking of Gelatin. *Biomacromolecules* **2004**, *5*, 1270–1279. DOI: 10.1021/bm034529a

- (44) Dinh, T. N.; Hou, S.; Park, S.; Shalek, B. A.; Jeong, K. J. Gelatin Hydrogel Combined with Polydopamine Coating To Enhance Tissue Integration of Medical Implants. *ACS Biomater. Sci. Eng.* **2018**, *4*, 3471-3477. DOI: 10.1021/acsbiomaterials.8b00886
- (45) Shin, S. R.; Aghaei-Ghareh-Bolagh, B.; Dang, T. T.; Topkaya, S. N.; Gao, X.; Yang, S. Y.; Jung, S. M.; Oh, J. H.; Dokmeci, M. R.; Tang, X. S.; Khademhosseini, A. Cell-Laden Microengineered and Mechanically Tunable Hybrid Hydrogels of Gelatin and Graphene Oxide. *Adv. Mater.* **2013**, *25*, 6385–6391. DOI: 10.1002/adma.201301082
- (46) Zhu, M.; Wang, Y.; Ferracci, G.; Zheng, J.; Cho, N. J.; Lee, B. H. Gelatin Methacryloyl and Its Hydrogels with an Exceptional Degree of Controllability and Batch-to-Batch Consistency. *Sci. Rep.* **2019**, *9*, 6863. DOI: 10.1038/s41598-019-42186-x
- (47) Dimatteo, R.; Darling, N. J.; Segura, T. In Situ Forming Injectable Hydrogels for Drug Delivery and Wound Repair. *Adv. Drug Delivery Rev.* **2018**, *127*, 167–184. DOI: 10.1016/j.addr.2018.03.007
- (48) Truong, V. X.; Ablett, M. P.; Richardson, S. M.; Hoyland, J. A.; Dove, A. P. Simultaneous Orthogonal Dual-Click Approach to Tough, *In-Situ* -Forming Hydrogels for Cell Encapsulation. *J. Am. Chem. Soc.* **2015**, *137*, 1618–1622. DOI: 10.1021/ja511681s
- (49) Chaudhuri, O.; Gu, L.; Klumpers, D.; Darnell, M.; Bencherif, S. A.; Weaver, J. C.; Huebsch, N.; Lee, H. P.; Lippens, E.; Duda, G. N.; Mooney, D. J. Hydrogels with Tunable Stress Relaxation Regulate Stem Cell Fate and Activity. *Nat. Mater.* **2016**, *15*, 326–334. DOI: 10.1038/nmat4489.

- (50) Swartzlander, M. D.; Blakney, A. K.; Amer, L. D.; Hankenson, K. D.; Kyriakides, T. R.; Bryant, S. J. Immunomodulation by Mesenchymal Stem Cells Combats the Foreign Body Response to Cell-Laden Synthetic Hydrogels. *Biomaterials* **2015**, *41*, 79–88. DOI: 10.1016/j.biomaterials.2014.11.020
- (51) Renner, P.; Eggenhofer, E.; Rosenauer, A.; Popp, F. C.; Steinmann, J. F.; Slowik, P.; Geissler, E. K.; Piso, P.; Schlitt, H. J.; Dahlke, M. H. Mesenchymal Stem Cells Require a Sufficient, Ongoing Immune Response to Exert Their Immunosuppressive Function. *Transplant*. *Proc.* **2009**, *41*, 2607–2611. DOI: 10.1016/j.transproceed.2009.06.119
- (52) Chen, S.; Shi, J.; Zhang, M.; Chen, Y.; Wang, X.; Zhang, L.; Tian, Z.; Yan, Y.; Li, Q.; Zhong, W.; Xing, M.; Zhang, L.; Zhang, L. Mesenchymal Stem Cell-Laden Anti-Inflammatory Hydrogel Enhances Diabetic Wound Healing. *Sci. Rep.* **2015**, *5*. DOI: 10.1038/srep18104
- (53) Kim, D. S.; Jang, I. K.; Lee, M. W.; Ko, Y. J.; Lee, D. H.; Lee, J. W.; Sung, K. W.; Koo, H. H.; Yoo, K. H. Enhanced Immunosuppressive Properties of Human Mesenchymal Stem Cells Primed by Interferon-γ. *EBioMedicine* **2018**, *28*, 261–273. DOI: 10.1016/j.ebiom.2018.01.002
- (54) Mao, A. S.; Özkale, B.; Shah, N. J.; Vining, K. H.; Descombes, T.; Zhang, L.; Tringides,
  C. M.; Wong, S. W.; Shin, J. W.; Scadden, D. T.; Weitz, D. A.; Mooney, D. J. Programmable
  Microencapsulation for Enhanced Mesenchymal Stem Cell Persistence and Immunomodulation.
  Proc. Natl. Acad. Sci. U. S. A. 2019, 116, 15392–15397. DOI: 10.1073/pnas.1819415116.
- (55) García, J. R.; Quirós, M.; Han, W. M.; O'Leary, M. N.; Cox, G. N.; Nusrat, A.; García, A. J. IFN-γ-Tethered Hydrogels Enhance Mesenchymal Stem Cell-Based Immunomodulation and Promote Tissue Repair. *Biomaterials* **2019**, *220*, 119403. DOI: 10.1016/j.biomaterials.2019.119403.

(56) Ghannam, S.; Bouffi, C.; Djouad, F.; Jorgensen, C.; Noël, D. Immunosuppression by Mesenchymal Stem Cells: Mechanisms and Clinical Applications. *Stem Cell Research and Therapy* **2010**, *I*, 1. DOI: 10.1186/scrt2.

# Table of Contents Graphic

